Resonant Phenomena in Conductor-Backed Coplanar Waveguides (CBCPW's)

Wen-Teng Lo, *Student Member, IEEE*, Ching-Kuang C. Tzuang, *Senior Member, IEEE*, S.-T. Peng, *Fellow, IEEE*, Ching-Cheng Tien, Chung-Chi Chang, and Jenq-Wen Huang, *Student Member, IEEE*

Abstract—**This paper presents a thorough and systematic investigation of resonant phenomena in conductor-backed coplanar waveguides (CBCPW's). We used a full-wave analysis first to establish benchmark results and a series of measurements have been conducted to confirm the theoretical results. As many as ten structures of different side-plane patterns were built and tested. All the test circuits exhibit many resonances over a frequency range, as measured in terms of two-port scattering parameters. Our full-wave analysis is capable of analyzing shielded guided-wave structures with finite-width substrate, and yields the scattering parameters of the coplanar waveguide circuits accounting for the overmoded-wave propagation. Finally, simple models are developed for physical understanding and interpretation of the resonant phenomena. When treating the side planes as patch resonators, we show that the resonant frequencies can be accurately estimated by this simple model. Followed by another MSL (microstrip-like) model, which considers the excitation of the first and the second MSL modes, the resonant frequencies thus obtained are also shown to be in very good agreement with measured results. By displaying the current distributions on the conductor strips in the through or resonant states of the test circuits, the MSL modes of resonances or the patch-type resonances can be clearly seen. When resonance occurs, the electromagnetic energy is confined or carried underneath the side planes and the signal energy can hardly propagate through the central signal line of the test circuit.**

I. Introduction

COPLANAR waveguide (CPW) and its variations such as conductor-backed coplanar waveguide (CBCPW) and uniplanar configuration, have been attractive transmission-line structures for monolithic microwave integrated circuits (MMIC) in that CPW's exhibit ease of parallel and series connection of both active and passive components [1]–[4]. However, the use of CPW subjects to many inherent limitations and many recent efforts have focused on the study of mode conversion at discontinuities in order to reduce undesirable propagation characteristics, such as the undesired modes of propagation, resonant phenomena in through-line measurements, and the leakage characteristics for various CPW configurations [5]–[16]. In circuit design, especially using the CPW-type structures, the effects of overmoding, leaky wave, and the undesired propagation modes must be avoided when broadband performance is desired. Furthermore, one often needs to mount the CPW circuit on a metal plate for packaging or testing, and the substrate and side planes of the CPW circuit are often of finite width. Therefore, we consider here, the general case of CBCPW with finite-width substrate and side planes, so that the ideas derived from this paper are not only of practical importance but also applied to other CPW cases as well.

In a CBCPW circuit with side planes of finite width, there exist three dominate modes that have no cutoff frequencies; they are the CPW mode, MSL, or coplanar microstrip (CPM) [7] mode, and the coupled slot-line mode. Without certain mode suppression techniques, these three dominant modes, as well as higher order modes, may be excited and propagate along the structures, resulting in the deterioration of circuit performance. The CBCPW test circuits studied in this paper possess lateral symmetry and we may, therefore, consider only the symmetric mode with a magnetic wall at the plane of bisection. Thus, only the effect of the microstrip-like modes will be investigated. The mode conversion at discontinuities assuming dominate CPW mode incidences had been discussed in [5]–[7]. In practice, the overmoded-wave propagation occurs when CPW circuit is fed at the substrate edge. Thus, it is our intent to investigate the wave propagation in the overmoded situation when the discontinuities exist at the substrate edge, and the theory presented in this paper may well be applied to the case discussed in [5]–[7]. It will be shown that even if the contribution of the microstrip-like mode is reduced [8], [9], the circuit performance will still deteriorate when certain boundary conditions are satisfied.

Until recently, the resonant phenomena of the CBCPW circuit has not been investigated with mutual verification between theory and experiment. In a preconditioned example [11], where a narrow CBCPW through line of finite-width substrate has its longitudinal dimension much greater than its cross-sectional geometry, the resonance observed in the S-parameter measurement is quantitatively related to the excitation of extra higher-order mode in the form of microstrip-like (MSL) mode. In this paper, we will present a viewpoint that the side planes of the CPW circuits always contribute to the resonance in a way

Manuscript received April 1, 1993; revised June 18, 1993. This work was supported by the National Science Council, Republic of China, under Grant NSC82-0404-D009-031 and NSC82-0404-D009-033.

W. T. Lo, C.-K. C. Tzuang, S. J. Peng, C.-C. Tien, and J.-W. Huang are with the National Chiao Tung University, Hsinchu, Taiwan.

C.-C. Chang is with Chung Shan Institute of Science and Technology (CSIST), Taoyuan, Taiwan.

IEEE Log Number 9212960.

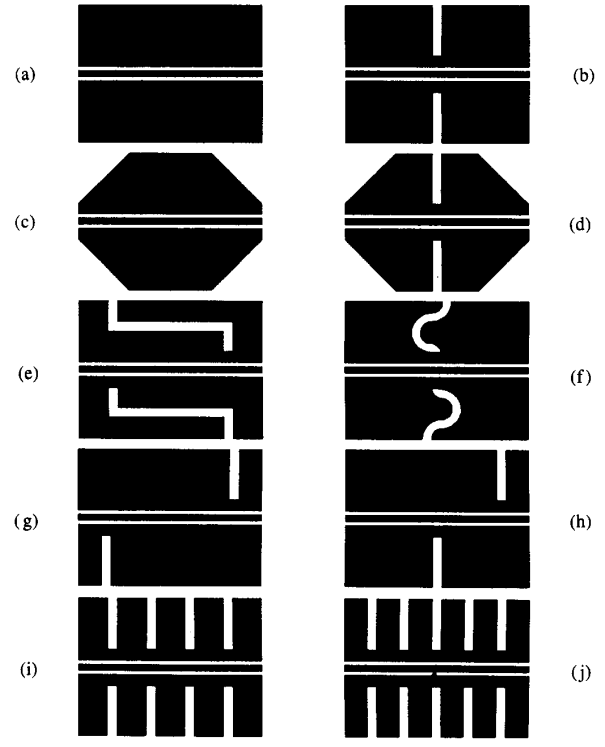

Fig. 1. The top views of the tested CBCPW through lines with different side-plane patterns.

similar to the planar circuit or patch antenna [17], [18]. In other words, the side planes act like two-dimensional resonators. Two examples shown in Figs. 1(a) and (b), for both theoretical and experimental studies, illustrate our viewpoint. To substantiate our viewpoint, other examples included in Fig. 1 are also investigated experimentally and the measured results show that the resonant phenomena still exist, though at different frequencies, regardless of side-plane patterns.

Parts (a) and (b) of Fig. 2 illustrate the top view and front view of the CBCPW through line as shown in Fig. 1(a). The ratio of l to s_P is fixed at 3 throughout this work. At reference planes a–a′ and b–b′ are two vertical conducting planes with two small holes allowing external connections to the Cascade MTF-26 test fixture. The 50 Ω CBCPW line has its dimensions and material parameters indicated in Fig. 2. In contrast, the structure in Fig. 3 exhibits the same 50 Ω CBCPW through line as shown in Fig. 2, except that the side planes have two cuts of width w_c along c–c'. The width w_p is wide enough so that the CBCPW is still very close to 50 Ω along the gap region c_1–c_2.

If only the CPW mode were excited, the transmission and reflection characteristics of CBCPW through lines shown in Fig. 1 (including Figs. 2 and 3) would exhibit almost identical responses. In practice, however, they are very different. In order to interpret such an unexpected result, a brief description of three-dimensional (3-D) full-

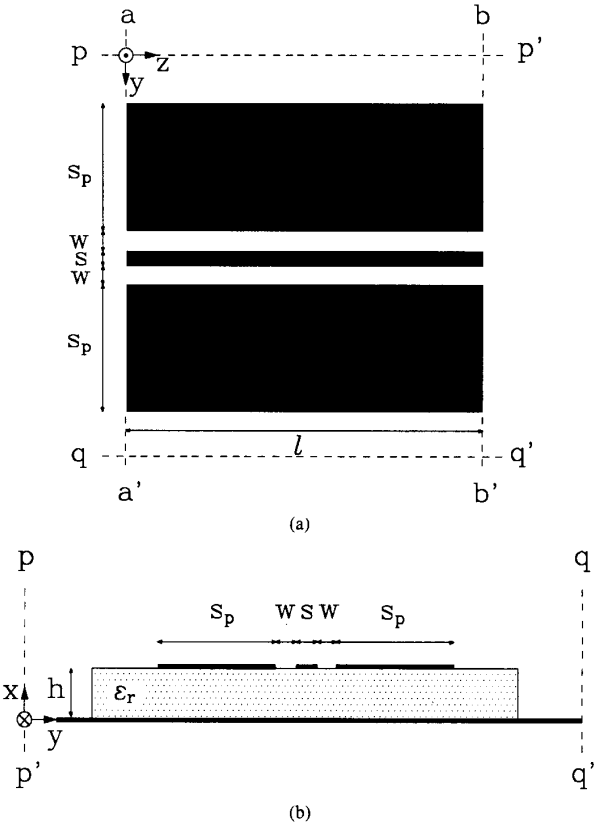

Fig. 2. The 50 Ω CBCPW through line of Fig. 1(a) with $l/s_p = 3.0$. The physical dimensions are $s = w = 0.508$ mm, $s_p = 6.0$ mm, and $l = 18.0$ mm. The material parameters are $\epsilon_r = 10.2$ and $h = 0.635$ mm. (a) Top view. (b) Front view.

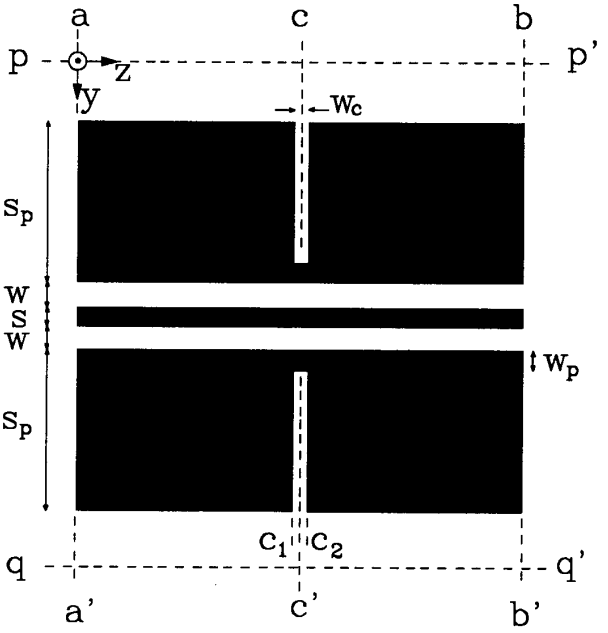

Fig. 3. The same 50 Ω CBCPW through line as that shown in Fig. 2 except that two cuts exist in the side planes. $w_c = 1.016$ mm, $w_p = 1.00$ mm.

wave techniques is given first in Section II. Comparisons of the measured and theoretic results of the two structures are then given in Section III. Section IV presents two simple models to predict the resonant frequencies associated with the structure in Fig. 2. Section V discusses the observed resonant phenomena of the two structures in terms of the current distributions on the central strip as well as side planes, as obtained by using the rigorous 3-D full-wave technique. This enables us to visualize how resonance works. Section VI shows the measured results for other CBCPW through lines shown in Fig. 1(c)–(j). Some conclusions are given in Section VII, along with a summary of the important results obtained in this paper.

II. Method of Analysis: A Full-Wave Space-Domain Integral Equation Approach Using Mixed-Potential Eigenfunction Expansion Technique

In contrast to the conventional full-wave formulations for CPW analyses, where the unknown variables for the Green's function are the slot electric field components, a new formulation extending from the mixed-potential mode-matching method described in [19], [20] is adopted in the present work to determine the unknown currents on the metal strips. Specifically, we consider here a generic planar transmission-line circuit on layered and non-layered substrates, which is the same as that shown in Fig. 1 of [20]. Referring to Fig. 2(b), the *TE*-to-*y* and *TM*-to-*y* Hertzian potentials are employed to obtain the *y*-directed eigenfunctions in the nonlayered region. All those layered regions incorporate *TE*-to-*x* and *TM*-to-*x* Hertzian potentials. Interested readers should refer to [19] for details. After some complicated numerical procedures we can obtain the electric field in terms of the surface conductor current as

$$\underline{E}_t = \boldsymbol{G} * \underline{J}_{(\text{tim.}+\text{tex.})} \tag{1}$$

where $\underline{E}_t$ is the tangential electric field vector, $\underline{J}_{(\text{tim.}+\text{tex.})}$ is the total surface current density vector composed of the impressed vector surface current density $\underline{J}_{(\text{tim.})}$ and the excited vector surface current density $\underline{J}_{(\text{tex.})}$, and $\boldsymbol{G}$ is the integral operator relating the surface current density to the electric field on the surface. On the conductor surface, (1) reduces to

$$\boldsymbol{G} * \underline{J}_{(\text{tex.})} = -\boldsymbol{G} * \underline{J}_{(\text{tim.})}. \tag{2}$$

Equation (2) is solved by applying the Galerkin procedure. The unknown surface current density $\underline{J}_{(\text{tex.})}$ is expanded by the rooftop basis function and the impressed current $\underline{J}_{(\text{tim.})}$ is applied at the boundary edge extended from the individual port. The procedure for extracting the *S* parameters of discontinuity problem is analogous to that introduced by Jansen [21]. Here, we extend this method to the analysis of CPW discontinuity problems when overmoded-wave propagation occurs. Fig. 4 shows the physical CPW discontinuity discussed in this paper. As shown in Fig. 4, the shaded regions are connected to ground, and Q_1 and Q_2 lay the impressed current. At a steady state, standing-wave current distribution is assumed in the regions D_1 and D_2, and thus we can extract the *S* parameters in these regions. RP_1 and RP_2 are the reference planes chosen to meet the practical measurement condition. The procedures for the *S*-parameter extraction are described as follows. Let the standing-wave current $I_{vu}(z)$ in regions D_1 and D_2 be approximated as

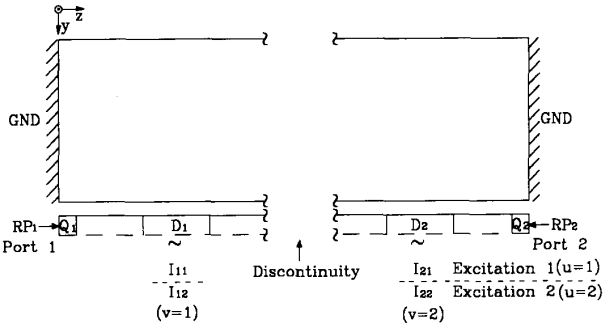

Fig. 4. Illustration of the *S*-parameter extraction regions for analyzing the discontinuity problem of CPW circuit.

$$I_{vu}(z) \cong I^{+}_{cvu}\, e^{-j\beta_{cv}z} - I^{-}_{cvu}\, e^{+j\beta_{cv}z} + I^{+}_{mvu}\, e^{-j\beta_{mv}z} - I^{-}_{mvu}\, e^{+j\beta_{mv}z} \qquad v, u = 1, 2 \tag{3}$$

where v is the index of a port and u is that of an excitation state. β_{cv} and β_{mv} are the propagation constants of the dominate CPW and MSL modes of Fig. 4 at port v. The above current is evaluated in region D_1 when $v = 1$ (port 1) and in D_2 when $v = 2$ (port 2). Since $I_{vu}(z)$ is known and obtained from the 3-D program, the current components I^{+}_{cvu}, I^{-}_{cvu}, I^{+}_{mvu}, and I^{-}_{mvu} can be readily solved. At reference point $z = z_{RPv}$, the total current I_{tvu} and total voltage V_{tvu} at port v and under the uth excitation state can then be calculated. Finally, the $2N$ port *Y*-matrix $[Y]$ and the *S*-parameter matrix $[S]$ are obtained by

$$[Y] = \begin{bmatrix} I_{t11} & I_{t12} \\ I_{t21} & I_{t22} \end{bmatrix} \begin{bmatrix} V_{t11} & V_{t12} \\ V_{t21} & V_{t22} \end{bmatrix}^{-1} \tag{4}$$

$$[S] = [Z_0]^{1/2}([Y_0] - [Y])([Y_0] + [Y])^{-1}[Y_0]^{1/2} \tag{5}$$

where $[Z_0]$ and $[Y_0]$ are diagonal matrices consisting of normalizing impedances and admittances at various ports, respectively. In this particular case under studied, $Z_{01} = Z_{02} = 100\ \Omega$.

As a direct result of the new attempt, the practical CBCPW structures with finite-width side planes and finite-width substrate as shown in Figs. 2 and 3, can be analyzed rigorously. In the following section we will compare the full-wave field-theoretic data obtained by the new formulation with the measured results for the structures shown in Figs. 2 and 3.

III. Comparison of Measured and Theoretic Scattering (*S*) Parameters

Two CBCPW circuits as shown in Figs. 2 and 3 have been built. The side planes of the two through lines at

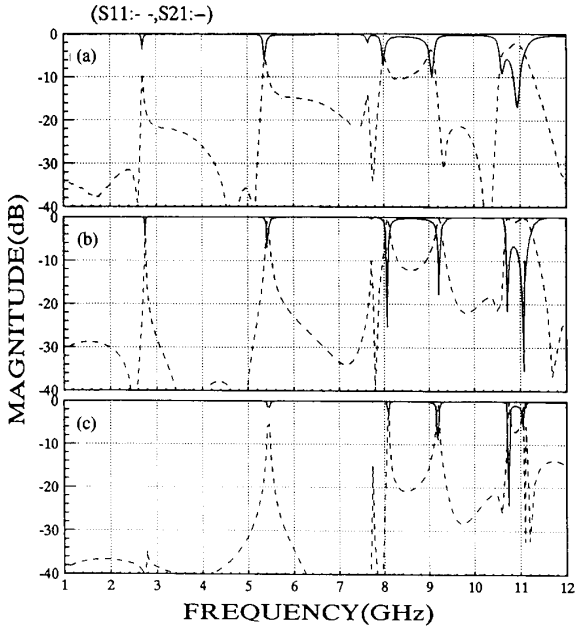

Fig. 5. The measured and theoretic transmission (S_{21}) and reflection (S_{11}) characteristics of the CBCPW through line shown in Fig. 2. (a) Measured results. (b) Theoretic results extracted by using CPW and MSL modes. (c) Theoretic results extracted by using CPW mode.

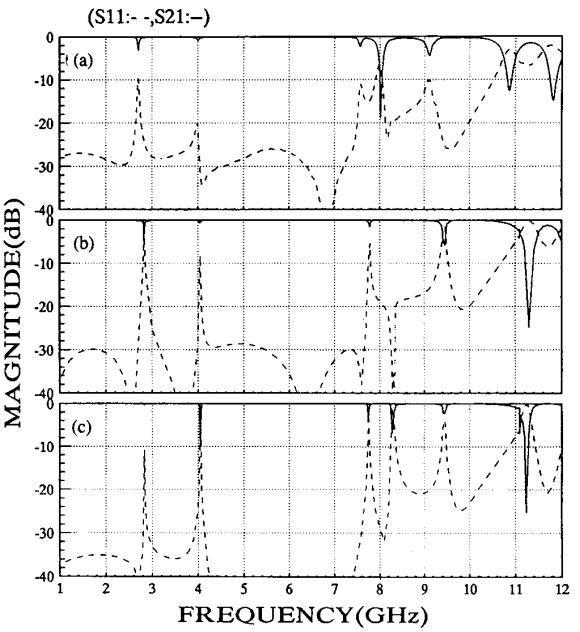

Fig. 6. The measured and theoretic transmission (S_{21}) and reflection (S_{11}) characteristics of the CBCPW through line shown in Fig. 3. (a) Measured results. (b) Theoretic results extracted by using CPW and MSL modes. (c) Theoretic results extracted by using CPW mode.

a-a' and b-b' are grounded by wrapping copper foil alongside the substrate vertical planes. This ensures good grounding at interfaces connected to the Cascade MTF-26 test fixture. The measured S parameters of the test circuits corresponding to Figs. 2 and 3 are shown in Figs. 5(a) and 6(a), respectively, from which the reflection coefficient S_{11} and the transmission coefficient S_{21} are observed to have 7 resonant peaks (dips) for S_{11} (S_{21}) for a 1–12 GHz frequency span. Figs. 5(b) and 6(b) are the corresponding theoretic results obtained by using the full-wave analysis described in the preceding section. As shown in Figs. 5(a) and (b), the theoretic results are in good agreement with the measured ones. The measured characteristics suffer from some conductor loss, dielectric loss, and also the radiation loss since the test circuits are built and measured without a conductor housing. The results in Figs. 6(a) and (b) show some deviation between measurement and theory. The discontinuity introduced by the slits in the side planes as shown in Fig. 3 complicates the analysis when compared to Fig. 2. Some useful experiences and general rules as described in [22] for selecting the number of expansion functions, should be exercised to give better theoretic results.

Figs. 5(c) and 6(c) are the theoretic results obtained as those of Figs. 5(b) and 6(b) except that we use only the dominant CPW mode in extracting the S parameters. Use of a single dominant CPW mode in S-parameter extraction gives the same resonant frequencies as those of using both dominant CPW and MSL modes. However, the latter shows much better results in the calculated S-parameter for a 1–12 GHz frequency span. Comparing the resonant positions of Figs. 2 and 3, the slits existing in the CBCPW through line do have certain impact on their relative positions of resonance. The first resonant point at 2.71 GHz is almost not affected by the cuts at the center of the side planes. The second resonance, however, is shifted drastically from 5.38 to 4.00 GHz by the cut that creates a slit in each of the side planes in Fig. 3. As we proceed along the frequency span, only the seventh resonance suffers more from the slit, e.g., from 10.94 to 11.81 GHz, and the rest of the resonances are only slightly affected. The observed resonance at 11.1 GHz appears in all of the theoretic plots while not shown in the measurement data of Figs. 5 and 6. This is due to the first waveguide mode excited in our theoretic analyses which assume that the test circuits are placed within the shielded transmission-line structures. More details about these discussions will be given in later sections.

IV. The Observed Resonances in Scattering (S)-Parameter Measurements: Patch (Antenna)-Resonator and MSL Models

It is already well known in [11] that the resonances will occur in the form of an extra higher-mode, i.e., the MSL mode, in a CBCPW through line which has a narrow-width side plane. In our test circuits shown in Figs. 2 and 3, the side plane is six times the width of that of [11]. Because the side plane is quite wide, the number of extra higher-order modes is more than one when frequency is below 12 GHz. Thus, we may extend our view of the one-dimensional resonator in [11] to the two-dimensional one in our present study. Table I lists the resonant frequencies

TABLE I
THE RESONANT FREQUENCIES AND THE CORRESPONDING MODES OBTAINED BY MEASUREMENT AND VARIOUS THEORETIC TECHNIQUES FOR CBCPW THROUGH LINE SHOWN IN FIG. 2

Resonant Phenomena nth Resonance #n (m_y, n_z)	Measurement	Patch-Resonator Model	MSL model; $m_y = 0, 1$; $\beta l = n_z \pi$; ($2N$-port Model, $m_y = 0$)	Obtained by 3-D Field-Theoretic Analysis
#1 (0, 1)	2.71	2.61	2.74(2.76)	2.76
#2 (0, 2)	5.38	5.22	5.40(5.44)	5.44
#3 (1, 1)	7.65	8.23	7.71(—)	7.75
#4 (0, 3)	8.01	7.83	8.04(8.08)	8.08
#5 (1, 2)	9.07	9.39	9.21(—)	9.22
#6 (0, 4)	10.61	10.44	10.67(10.71)	10.71
#7 (1, 3)	10.94	11.06	11.27(—)	11.08

Note: unit = GHz.

associated with the structure depicted in Fig. 2 obtained by measurement, patch-resonator model, MSL model, and a 3-D full-wave analysis. The third column of Table I lists the calculated resonant frequencies by considering the side planes as patch (antenna) resonators [17], [18]. In calculating these resonant frequencies, we neglect the effect of fringing fields of the side-plane conductor. The index appearing in the first column is modified by adding (m_y, n_z) parameters. When $m_y = 0$ and $n_z = 1, 2, \cdots$, etc., the resonance appears in the longitudinal direction (or z direction) with negligible field variation in the transverse plane (or y direction). When $m_y = 1$ and $n_z = 1$, the resonance should have one half-wave variation in either y or z direction. Such field description is well known in patch-resonator theory. When comparing the data shown in columns 2 and 3 of Table I, the agreement is fairly good except the third and fourth resonant positions, where a reverse order takes place in column 3. Nevertheless, the simple patch-resonator model does give the correct number of resonances and predicts where the resonance should occur with good accuracy in the frequency spectrum related to Fig. 2.

Given the fact that the observed resonances are closely related to patch-resonator-type resonances, we continue to model the resonant frequencies more accurately by another approach. This method extends a similar technique reported in [11] to estimate the resonant frequencies by obtaining the dispersive propagation constants of the extra higher-order modes, namely, the MSL modes. Resonances occur when the resonant condition (6) is satisfied, e.g.,

$$\beta_{MSL} l = n\pi \tag{6}$$

where β_{MSL} is the propagation constant of the dominant or higher-order microstrip-like mode.

Fig. 7 plots the dispersive propagation constants of infinite uniform coupled lines of magnetic-wall symmetry. The structural parameters are the same as those given in Figs. 2 and 3. The major difference between this paper and [11] is that there is an additional MSL mode above 6.7 GHz in our study. This extra MSL mode has one change-over of transverse electric field pattern underneath the side planes, resembling the odd-mode type of microstrip electric field distribution. Following the procedure reported in [11], we obtain the resonant frequencies listed in the fourth column of Table I. These resonant frequencies with $m_y = 1$ indicate that the second MSL mode just mentioned is taken into account. Now the agreement between theory and experiment is much better than what the previous patch-resonator model can offer. Those resonant frequencies inside the parentheses are obtained by the $2N$-port model of N-coupled transmission lines described in [11], assuming that $m_y = 0$. Again, the solutions for resonant frequencies are very close to the measured results. As stated in Section III, the resonant point occurring at 11.1 GHz is due to the first waveguide mode. This can be confirmed by using the resonant condition $\beta l = \pi$; here β now is the propagation constant of the first waveguide mode and l in the present study happens to be the dimension of the conductor housing along the z axis.

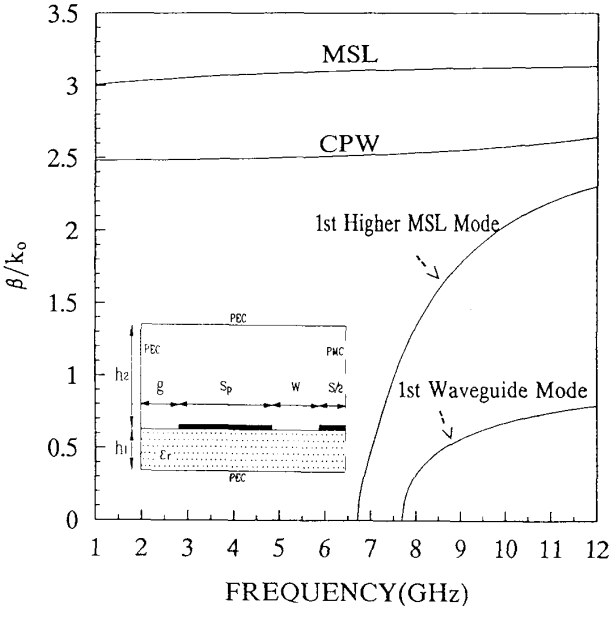

Fig. 7. The dispersive propagation constants of infinite uniform coupled lines of magnetic-wall symmetry. The structural parameters are $h_1 = 0.635$ mm, $h_2 = 9.365$ mm, $s_p = 6.0$ mm, $w = s = 0.508$ mm, $g = 3.238$ mm, and $\epsilon_r = 10.2$.

V. Visual Representation of Resonant Phenomena Using the Rigorous Three-Dimensional (3-D) Full-Wave Space-Domain Integral Equation Technique

Employing the rigorous 3-D full-wave technique described in Section II, we list the resonant frequencies of the structure shown in Fig. 2 in the fifth column of Table I, by sweeping the frequencies from 1 GHz to 12 GHz and carefully locate the resonant positions. As shown in Table I, the results obtained by the 3-D analyses are very close to those obtained by the MSL model assuming $m_y = 0$ and 1, and they are very close to the measured values. In the case of Fig. 3 where a slit exists in each of the side planes, the simple MSL model or patch-resonator model becomes cumbersome and only the method of employing the 3-D field-theoretic analysis can be used to calculate the resonant frequencies. The resonant frequencies obtained by measurement and theory differ by less than 4%.

As the validity of the 3-D analysis technique is established, we are able to visualize with confidence the resonant phenomena as illustrated in Figs. 5, 6, and Table I, which are still abstract to most investigators until now. With the aid of the full-wave 3-D program, the current distributions on the central signal line and side planes can be obtained. Knowing these current distributions, the though or resonant characteristics of the test circuits can be understood. For example, parts (a) and (b) of Fig. 8 plot the J_z and J_y components on the metal strips of Fig. 2 tested at 2.000 GHz. Note that the impressed source currents are assumed equal in magnitude and opposite in phase at input and output ports, respectively. Because of even symmetry, a magnetic wall is placed at $y = 10$ mm. On the central signal strip, a singular behavior is seen at the edge of the strip. Across the small gap, just opposite to the central line, there shows a current distribution out of phase to its counter part at the edge of the central line. This suggests that, in the through state of Fig. 2, the CPW mode dominates and results in very good transmission characteristics with measured return loss about 35 dB as shown in Fig. 5(a). When the first resonance occurs at 2.756 GHz (see Fig. 5(a) and Table I), most electromagnetic energy is carried by the side planes in the form of the MSL mode as seen in parts (a) and (b) of Fig. 9. Note that not only is the singular behavior at the edges of the side plane observed in Fig. 9(a), but the singularities are pointed toward the same direction along the z-axis. When resonance occurs, the MSL mode dominates and results in significant transmission loss in the through-line measurement. Figs. 10(a) and (b) illustrate an entirely different form of resonance from those shown in Figs. 9(a) and (b). A two-dimensional current variation in the y–z plane is seen. In Fig. 10(a), the J_z component varies from the most positive value toward the most negative value in all four sides. Fig. 10(b), on the other hand, depicts a basketlike type of current distribution. Both plots illustrate that a two-dimensional resonance occurs in the side planes

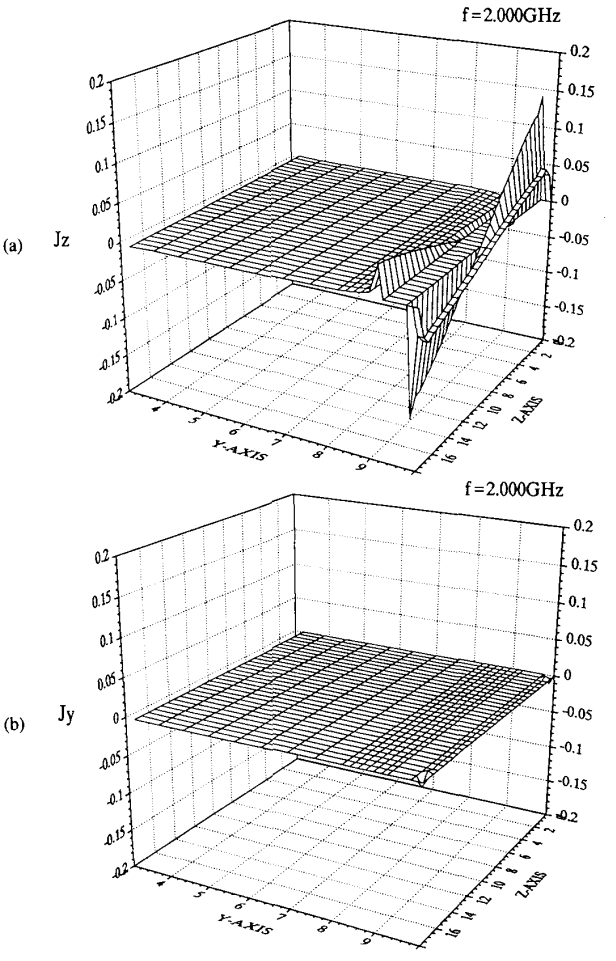

Fig. 8. Longitudinal (J_z) and transverse (J_y) current components at the through state of Fig. 2 at $f = 2.000$ GHz.

and such a resonance can be modeled by the second (higher) MSL mode as described in Section IV.

The effects of slits in the side planes of Fig. 3 on the (m_y, n_z) = (0, 1) and (1, 1) resonant modes, are illustrated in Figs. 11 and 12, respectively. For the (0, 1) resonant mode, the slits do not stop the resonance but shift the resonant frequency upward by 0.067 GHz from 2.756 GHz in Fig. 9 to 2.823 GHz in Fig. 11. Parts (a) and (b) of Fig. 11 also show that the current distributions J_z and J_y are similar to those shown in Fig. 9, except that they are perturbed by the slits in the middle of the side planes. As a result, we still attribute this resonant mode as the (0, 1) mode. Note that the transverse current component J_y flows toward the y-axis with two singularities nearby the slit. Nevertheless in the state of resonance, very little energy is carried away by the central signal line. Similarly, the effect of slits on the (1, 1) resonant mode is illustrated in Fig. 12. Comparing Figs. 12(a) and (b) to Figs. 10(a) and (b), the slits only perturb the current distributions shown in Figs. 10(a) and (b) and result in a slight increase of resonant frequency.

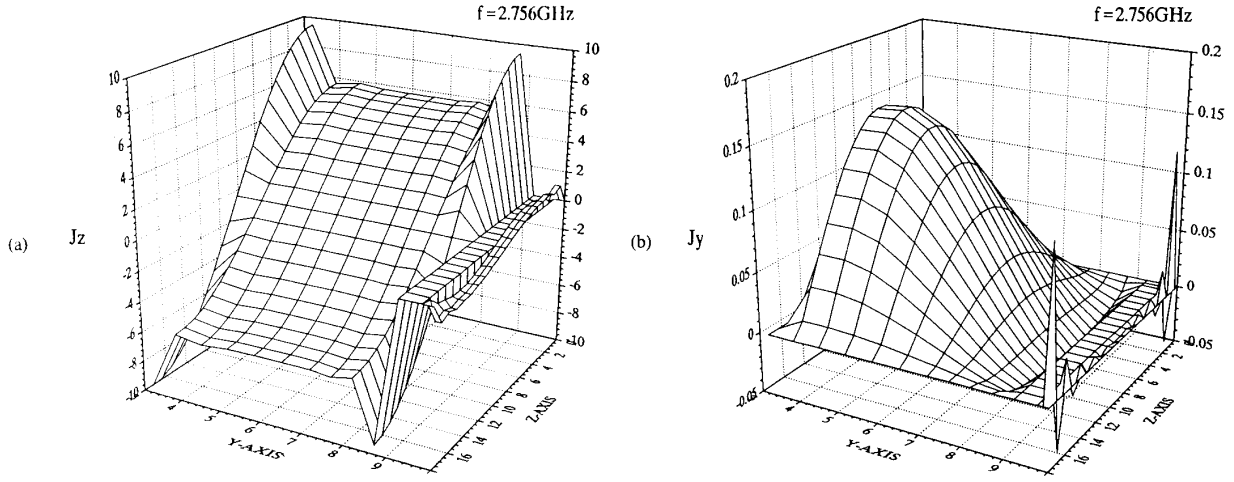

Fig. 9. Longitudinal (J_z) and transverse (J_y) current components at the resonant state (0, 1) mode, of Fig. 2 at f = 2.756 GHz.

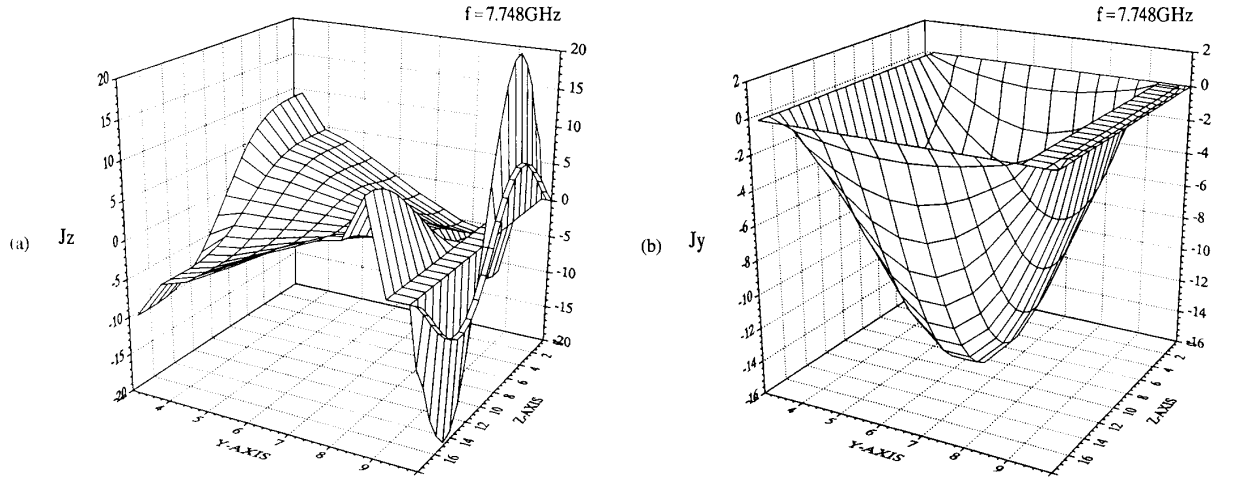

Fig. 10. Longitudinal (J_z) and transverse (J_y) current components at the resonant state (1, 1) mode, of Fig. 2 at f = 7.748 GHz.

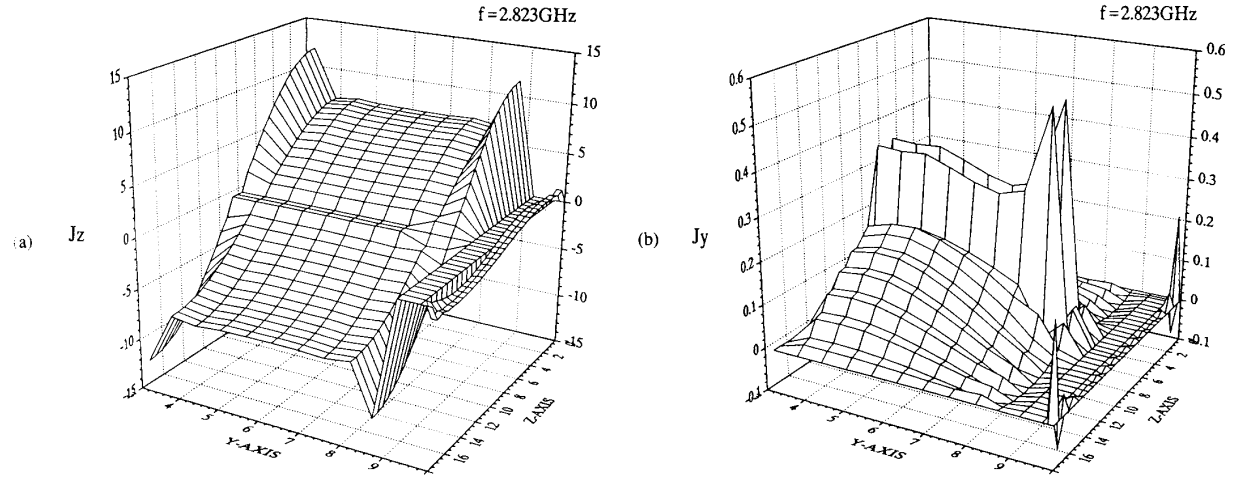

Fig. 11. Longitudinal (J_z) and transverse (J_y) current components at the resonant state (0, 1) mode, of Fig. 3 at f = 2.823 GHz.

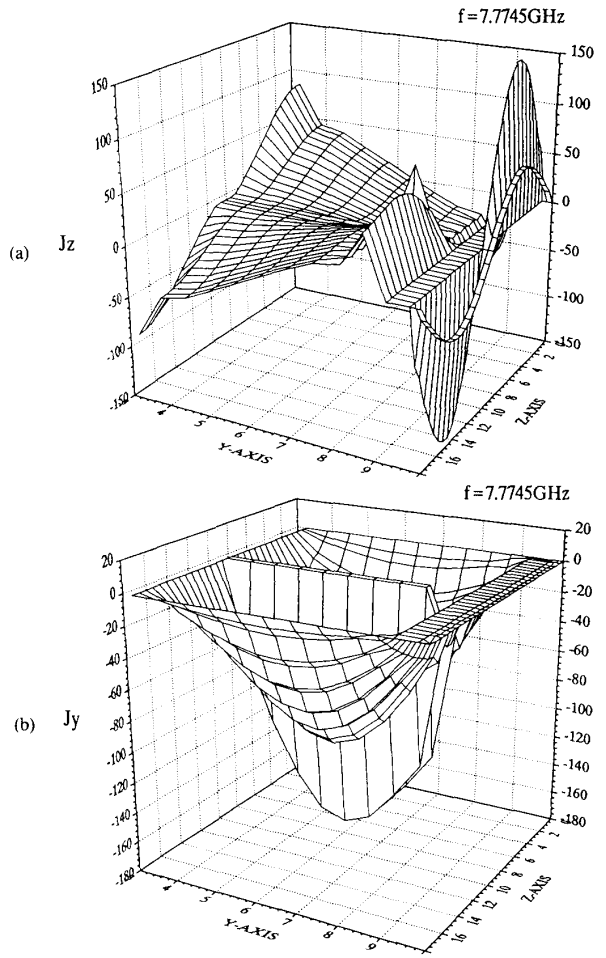

Fig. 12. Longitudinal (J_z) and transverse (J_y) current components at the resonant state (1, 1) mode, of Fig. 3 at f = 7.7745 GHz.

VI. Measured Results for Other CBCPW Through Lines Shown in Fig. 1(c)-(j)

As discussed in the previous sections, when the CBCPW through line operates at resonant frequencies, most of the electromagnetic energy is confined or carried underneath the side planes in the form of MSL modes and the signal energy can hardly propagate through the central signal line. These resonant frequencies can be altered by the side-plane geometry. Fig. 13 shows the measured results for the other eight CBCPW through lines with different side-plane patterns defined by Fig. 1(c)-(j). The most important fact shown in Fig. 13 is that there are many, at least five, typically seven, resonant frequencies still observed even when the similar technique for suppressing the TE_{01} mode in a rectangular waveguide by using the slits [23] is employed here. This implies that the so-called MSL modes still propagate in the CBCPW circuits and the modified side-plane patterns cannot stop resonances which are due to the overmoded excitation. In practice, the suppression of the undesired propagation

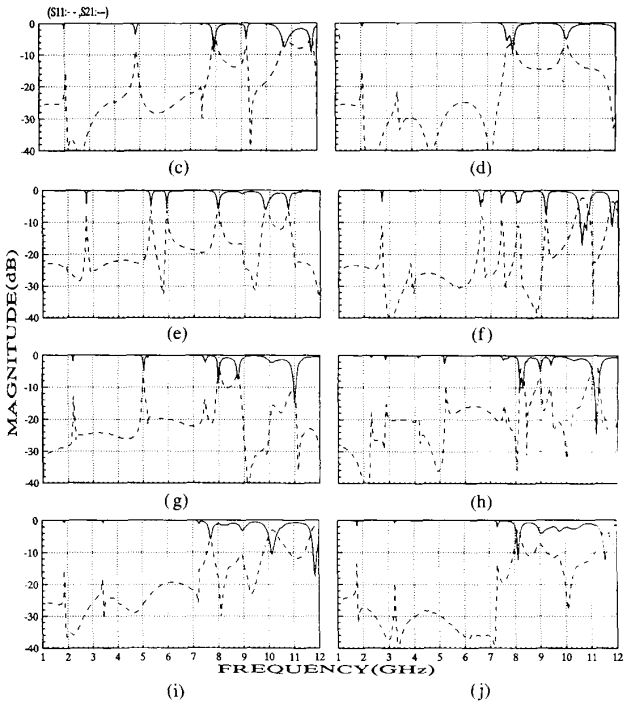

Fig. 13. The measured results for the other CBCPW through lines with different side-plane patterns defined by Fig. 1(c)-(j).

modes, namely, the coupled slot-line mode and microstrip-like mode, is often necessary when broadband performance is desired. If air bridges or via holes are introduced along with the slot lines to reduce the undesired propagation modes, the spatial intervals between these resultant discontinuities should be designed carefully so as not to create the resonant condition, for example, (6) for the case of two via holes.

VII. Conclusion

The resonant phenomena in CBCPW through-line circuits are investigated both experimentally and theoretically. A rigorous three-dimensional full-wave space-domain integral equation method accompanied by the S-parameter extraction technique are utilized for the analysis of the CPW discontinuity problems. The patch-resonator model and the MSL model are employed to understand the origin of resonance existing in the test circuit shown in Fig. 2. The 3-D program is also invoked by displaying the current distributions to help visualize how the CBCPW test circuits work at both through and resonant states. The results thus obtained, validate the conclusions drawn by the patch-resonator model and the MSL model. The resonant phenomena reported in the paper can be attributed to one-dimensional (Figs. 9 and 11) or two-dimensional (Figs. 10 and 12) resonances regardless of the presence of the slits shown in all the case studies, Fig. 1(b)-(j). Unless some means of suppressing the resonant phenomena are exercised, the CBCPW MMIC or hybrid MIC would experience certain resonances and they should be designed with extreme caution.

REFERENCES

[1] M. Riaziat, I. Zubeck, S. Bandy, and G. Zdasiuk, "Coplanar waveguides used in 2–18 GHz distributed amplifier," in *IEEE MTT-S Int. Microwave Symp. Dig.*, June 1986, pp. 337–338.

[2] D. Neuf and S. Spohrer, "Double balanced, coplanar, image rejection mixer uses monolithic MESFET QUAD," in *IEEE MTT-S Int. Microwave Symp. Dig.*, 1991, pp. 843–846.

[3] M. Riaziat, E. Par, G. Zdasiuk, S. Bandy, and M. Glenn, "Monolithic millimeter-wave CPW circuits," in *IEEE MTT-S Int. Microwave Symp. Dig.*, 1989, p. 525–528.

[4] M. Muraguchi, T. Hirota, A. Minakawa, K. Ohwada, and T. Sugeta, "Uniplanar MMIC's and their applications," *IEEE Trans. Microwave Theory Tech.*, vol. MTT-36, pp. 1896–1901, Dec. 1988.

[5] R. W. Jackson, "Considerations in the use of coplanar waveguide for millimeter-wave integrated circuits," *IEEE Trans. Microwave Theory Tech.*, vol. MTT-34, pp. 1450–1456, Oct. 1986.

[6] —, "Mode conversion due to discontinuities in modified grounded coplanar waveguide," in *IEEE MTT-S Int. Microwave Symp. Dig.*, 1988, pp. 203–206.

[7] —, "Mode conversion at discontinuities in finite-width conductor-backed coplanar waveguide," *IEEE Trans. Microwave Theory Tech.*, vol. MTT-37, pp. 1582–1589, Oct. 1989.

[8] M. Riaziat, I. J. Feng, R. Majidi-Ahy, and B. A. Auld, "Single-mode operation of coplanar waveguides," *IEEE Electron. Device Lett.*, vol. EDL-23, pp. 1281–1283, Nov. 1987.

[9] M. Riaziat, R. Majidi-Ahy, and I. J. Feng, "Propagation modes and dispersion characteristics of coplanar waveguides," *IEEE Trans. Microwave Theory Tech.*, vol. 38, pp. 245–251, Mar. 1990.

[10] M. A. Magerko, L. Fan, and K. Chang, "Multiple dielectric structures to eliminate moding problems in conductor-backed coplanar waveguide MIC's," *IEEE Microwave and Guided Wave Lett.*, vol. 2, pp. 257–259, June 1992.

[11] C.-C. Tien, C.-K. C. Tzuang, S.-T. Peng, and C.-C. Chang, "Transmission characteristics of finite-width conductor-backed coplanar waveguide," *IEEE Trans. Microwave Theory Tech.*, Special Issue on Modeling and Design of CMMIC's, Sept. 1993.

[12] W.-T. Lo, C.-K. C. Tzuang, S.-T. Peng, C.-C. Chang, J.-W. Huang, and C.-C. Tien, "Resonant phenomena in conductor-backed coplanar waveguide (CBCPW)," in *IEEE MTT-S Int. Microwave Symp. Dig.*, 1993, pp. 1199–1202.

[13] H. Shigesawa, M. Tsuji, and A. A. Oliner, "Conductor-backed slot line and coplanar waveguide: Dangers and full-wave analyses," in *IEEE MTT-S Int. Microwave Symp. Dig.*, 1988, pp. 199–202.

[14] —, "A new mode-coupling effect on coplanar waveguides of finite width," in *IEEE MTT-S Int. Microwave Symp. Dig.*, 1990, pp. 1063–1066.

[15] M. Tsuji, H. Shigesawa, and A. A. Oliner, "New surface-wave-like mode on CPWs of infinite width and its role in explaining the leakage cancellation effect," in *IEEE MTT-S Int. Microwave Symp. Dig.*, 1992, pp. 495–498.

[16] M. Tsuji and H. Shigesawa, "The feature of the narrow-pulse transmission on conventional coplanar waveguides when power leakage is present," in *IEEE MTT-S Int. Microwave Symp. Dig.*, June 1992, pp. 991–994.

[17] K. C. Gupta, R. Garg, and R. Chadha, *Computer-Aided Design of Microwave Circuits*, Chap. 8. New York: Artech House, 1981.

[18] Y. T. Lo, D. Solomon, and W. F. Richards, "Theory and experiment on microstrip antennas," *IEEE Trans. Antennas and Propagation*, vol. AP-27, pp. 137–145, Mar. 1979.

[19] C.-K. C. Tzuang and J.-D. Tseng, "A full-wave mixed potential mode-matching method for the analysis of planar or quasi-planar transmission lines," *IEEE Trans. Microwave Theory Tech.*, vol. 39, pp. 1701–1711, Oct. 1991.

[20] W.-T. Lo and C.-K. C. Tzuang, "A new full-wave integral equation method for the analysis of coplanar strip circuit using the mixed-potentials eigenfunction expansion technique," in *IEEE MTT-S Microwave Symp. Dig.*, 1993, pp. 1539–1542.

[21] R. H. Jansen and W. Wertgen, "Modular source-type 3D analysis of scattering parameters for general discontinuities, components and coupling effects in (M)MICs," in *17th European Microwave Conf. Proc.*, 1987, pp. 427–432.

[22] *LINMIC+/N User Manual*, 1992. Jansen Microwave, Ratingen, Germany.

[23] T. Koryu Ishii, *Microwave Engineering*, Second Edition, Chap. 6. Harcourt Brace Jovanovich, Inc.

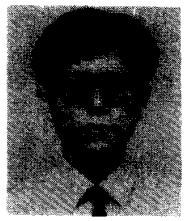

Wen-Teng Lo (S'90) was born in Taiwan on December 6, 1965. He received the B.S. degree in electronic engineering and the Ph.D. degree from the National Chiao Tung University, Hsinchu, Taiwan, in 1988 and 1993, respectively. He currently conducts various research and development programs on wireless communication circuits and systems. His research interests include the analysis and design of microwave and millimeter-wave components.

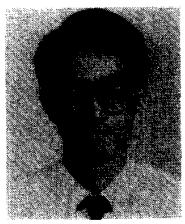

Ching-Kuang C. Tzuang (S'84–M'86–SM'92) was born in Taiwan on May 10, 1955. He received the B.S. degree in electronic engineering from the National Chiao Tung University, Hsinchu, Taiwan, in 1977, the M.S. degree from the University of California at Los Angeles, in 1980, and the Ph.D. degree in electrical engineering from the University of Texas at Austin, in 1986, where he worked on high-speed transient analyses of monolithic microwave integrated circuits.

From February 1981 to June 1984, he was with TRW, Redondo Beach, CA, working on analog and digital monolithic microwave integrated circuits. Since September 1986, he has been with the Institute of Communication Engineering, National Chiao Tung University, Hsinchu, Taiwan. His research activities involve the design and development of millimeter-wave and microwave active and passive circuits and the field theory analysis and design of various quasi-planar integrated circuits.

S. T. Peng (M'74–SM'82–F'88) was born in Taiwan, on February 19, 1937. He received the B.S. degree in electrical engineering from the National Cheng Kung University, in 1959, the M.S. degree in electronics from the National Chiao Tung University, in 1961, both in Taiwan, and the Ph.D. degree in electrophysics from the Polytechnic Institute of Brooklyn, Brooklyn, NY, in 1968.

After 1968, he held various research positions with the Polytechnic Institute of Brooklyn. From 1983 to 1990, he was a Professor of Electrical Engineering and Director of the Electromagnetics Laboratory at the New York Institute of Technology, Old Westbury, NY. Since 1991, he has been a Professor of Communication Engineering at the National Chiao Tung University, Taiwan. He has been active in the field of wave propagation, radiation, diffraction, and nonlinear electromagnetics, and has published numerous papers on electromagnetics, optics, and acoustics.

Dr. Peng is a member of Sigma Xi.

Ching-Cheng Tien was born in Taiwan, on March 19, 1966. He received the B.S. degree in communication engineering from the National Chiao Tung University, Hsinchu, Taiwan, in 1988 and the Ph.D. degree at the same University, in 1993. His current research interests include the analysis and design of microwave and millimeter-wave components.

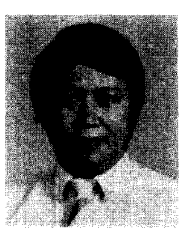

Chung-Chi Chang was born in Shanghai, China, in 1946. He received the B.S. and M.S. degrees in electronic engineering from Chun Cheng Institute of Technology, Taoyun, Taiwan, in 1970 and 1975, respectively, and Ph.D. degree from Southern Methodist University, Dallas, Texas, in 1982.

From 1975 to 1979, he was an Assistant Researcher at the Electronic System Division, Chung Shan Institute of Science and Technology (CSIST), Taiwan. There he was responsible for design, fabrication, and testing of hybrid micro-

wave integrated circuits. After he received the Ph.D. degree, he returned to CSIST and worked as an Associate Researcher in manufacturing both thin film and thick film hybrid integrated circuits. Since 1986, he has been in charge of the Solid State Device Section at CSIST. He has also worked as a part-time Associate Professor at National Chiao Tung University, Hsinchu, Taiwan, since 1989.

Dr. Chang's interests include semiconductor devices, components, circuit modules, high-power PIN diodes, HEMT's, photonic devices, microwave circuit modules, frequency synthesizers, and SMT's.

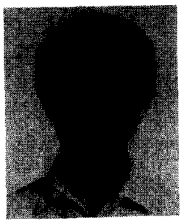

Jenq-Weng Huang (S'91) was born in Taiwan on March 17, 1963. He received the B.S. degree in electronic engineering from the Feng Chia University, Taichung, Taiwan, in 1985 and the M.S. degree in communication engineering from the National Chiao Tung University, Hsinchu, Taiwan, in 1991, where he is currently working towards the Ph.D. degree.

From 1987 to 1989, he was a teaching assistant at Shu-Te Institute of Technology. His research interests include the microwave and millimeter-wave integrated circuit design.